Single molecule studies of the bacterial curli protein CsgA reveal a structurally dynamic monomeric structure

Daniel A.N. Foster, Derek R. Dee.

Food, Nutrition and Health, Faculty of Land and Food Systems, The University of British Columbia, 2205 East Mall, Vancouver, BC, V6T 1Z4, Canada

For correspondence: Derek.Dee@ubc.ca

Abstract

Functional amyloid forms the scaffold that supports bacterial communities, making them an important antimicrobial target. In particular, the subunit of curli fibrils, CsgA, has recently had its fibril assembly deciphered by cryoEM. However, the folding of CsgA has yet to be careful examined. We report the first *in vitro* single molecule folding trajectories of CsgA, constituting two principal modes: discrete and non-piecewise unfolding reflective of the assembly of R domains, and a blend of metastable states or of a molten globule. Moreover, extending refolding time to many seconds does not obstruct the appearance of metastable states. In order to restrain the aggregation propensity of this protein, we developed an assay to trigger native folding of CsgA under controlled conditions in a microfluidic flow cell. From there we measured the individual folding trajectories of single molecules of CsgA using force spectroscopy by optical tweezers. This work exploits an engineered disulfide trap in the protein, where native folding becomes possible after reduction of the cysteine substitutions. When folding, CsgA does not get locked into a β-hairpin assembly, by can be found in a metastable state in about a quarter of the incidences in which it is probed.

Introduction

A biofilm serves as a bacterial community's home, protecting against environmental stressors such as antibiotics. The functional amyloid known as curli, present in *E. coli* biofilms, is one of the best studied amyloidal systems. CsgA is the subunit of these curli fibers, though there are many folding chaperones and inhibitors involved in its synthesis pathway. However, atomistic details of fibril assembly and the CsgA amyloid structure remain unresolved. Progress in understanding CsgA's structure has come from modelling and cryoEM, among other techniques. Monomeric CsgA has long been described as intrinsically disordered (*1*) and is known to be highly prone to aggregation, confounding high-resolution studies at the ensemble level. Single molecule force spectroscopy (SMFS) is well placed to elucidate the folding pathway of CsgA, and resolve the minutia of CsgA's assembly into amyloid by resolving the protein's behaviour that is hidden within ensemble averaging.

Curli accounts for 85% of the matrix materials in curli-related biofilms (*2*). It organises into aggregates with their beta-sheet structures aligned perpendicular to the long fibril-axis (cross-β architecture) (*3*), forming amyloid. These fibrils are thermodynamically stable, capable of self-propagation, have a high aspect ratio (*e.g.* 10-20 nm wide and 10^2-10^3 nm long), provide high mechanical strength (*4*) and are protease resistant (*5–8*). Given amyloid's key role in the

scaffolding of biofilm, it is not surprising that such amyloidal proteins are highly conserved across genera (*9*, *10*). Thus, to further development of novel anti-biofilm/anti-bacterial treatments (*11*) a detailed understanding of the molecular basis the amyloid structure is needed.

The curli proteins from *E. coli* are the best characterised bacterial amyloid system. Six proteins encoded by curli-specific genes (csg) play a unique role in the tightly controlled process of CsgA fibril synthesis (Figure 1). Aggregation of the intrinsically disordered protein (IDP) CsgA is nucleated at the outer cellular membrane by CsgB (*12*), but cytotoxic aggregates are inhibited in the periplasm by chaperone proteins CsgC and CsgH (*13*, *14*). The secretion of CsgA to the outer membrane is controlled by CsgG, CsgE and CsgF (*15*), where CsgB nucleates CsgA fibril formation (*16*). CsgF is anchored to the outer membrane and may anchor CsgB to the membrane (*17*). Currently, most of the mechanistic details are unknown (*2*, *16*, *18*), such as the dynamic structure of CsgA or CsgB monomers, how CsgB nucleates CsgA amyloid formation, or how CsgC, CsgE and CsgH inhibit fibril formation (*2*, *14*).

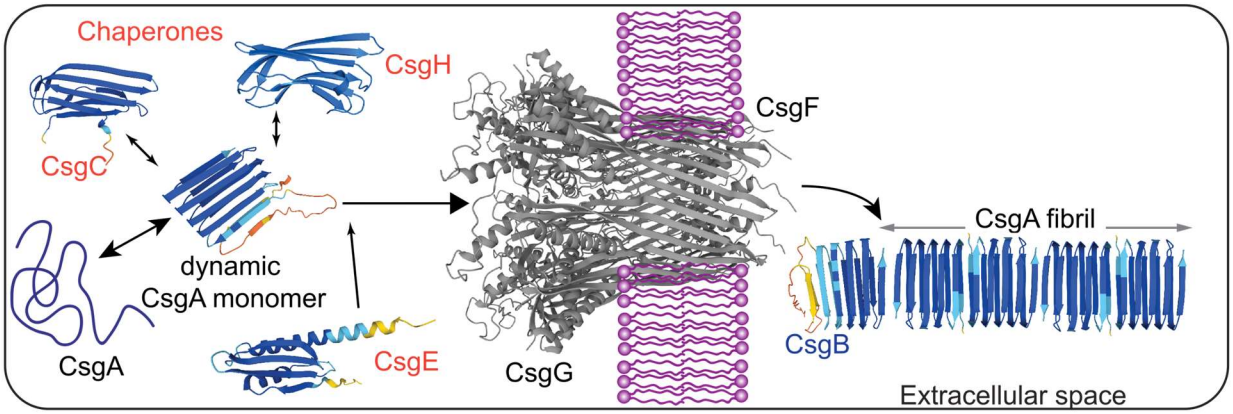

Figure 1 **Overview of regulated CsgA amyloid formation**. Solubility of CsgA in the periplasm is maintained by CsgC and CsgH amyloid inhibitors while it is exported out of the cell through the CsgG-CsgF β-barrel pore complex in the outer membrane, for incorporation into fibrils with CsgB acting as a nucleator for biofilm supporting scaffolds.

Progress towards the amyloid structure has been made recently through cryoEM imaging of a CsgA R-domain analogue (*19*) and with an engineered CsgA with residue substitutions to control aggregation onset (*20*). Ensemble studies of CsgA do not presume a fixed R-repeat structures, rather, indications from circular dichroism spectra measurements point towards CsgA as unstructured (*21*). Moreover, cryoEM structures raise questions about monomer orientation within the amyloid fibril (*22*). Some protein-fusion CsgA magnetic tweezers measurements have been published (*23*), claiming piecewise unfolding based on a few traces.

Why single molecule experiments? Rare or transient subpopulations are averaged out in ensemble measurements. To understand the folding pathways comprehensively, we leverage optical tweezers (OT) for *in vitro* measurements, while controlling the onset of the CsgA folding with an engineered disulfide reduction trigger. OT measurements of IDPs linked to disease amyloid (*such as the prion and α-synuclein proteins*) have established the type of results that can be expected from this mode of investigation (*24–26*).

The structure of CsgA amyloid currently has two cryoEM reconstructions. Sleutel *et al.* took a wide-ranging view of CsgA analogues in bacteria and opted for a 15.5 R repeat structure (*19*). Our colleagues made use of the internal cysteine amino acid change CsgA protein (A63C/V140C) developed by the Chapman lab (*27*), allowing fibrillation to be turned on by reducing agent [PDB: 8ENR]. Preceding these structural determinations, foundational modelling work was done by DeBenedictis *et al.*, examining the results of structural predictions and their stability under molecular dynamics simulations out to 150 ns (*28*). Since that time, webservers are now available to the public for structure prediction, such as Robetta (*29*) (using *de novo* structure prediction methods) and AlphaFold 3 (AF3; using machine learning based on the records of the PDB), which together predict similar CsgA structures. Conversely, bulk studies show that these proteins are ostensibly disordered, and importantly, the deep learning methods are biased from sampling amyloid fragments that crystallise well. The β-hairpin solenoid shown by DeBenedictis *et al.* is replicated in the machine learning results.

A homologue of CsgA/curli in *Pseudonomas*: FapC, has recently had a cryoEM structure published(*30*). Similarly to CsgA, FapC has imperfect repeats (R1 to R3, ~ 30 residues per repeat) that participate in β-sheet alignment in fibril formation, but in a 3-layer β-solenoid. Hansen *et al*. report that in-solution nuclear magnetic resonance provided secondary structure indicators for FapC, but otherwise the protein is shown to be intrinsically disordered. They used all-atom molecular dynamics simulations to inform cryoEM structure reconstruction.

In the case of CsgA, the sequence of 22 residues on the N-terminus (N22; after signal peptide removal) is generally predicted as unstructured or containing β-sheet regions, while the modelling used for the cryoEM structure (*20*) presumed this sequence to be unstructured. For the structure reconstruction during cryoEM, which is an endpoint ensemble average, the N22 was assumed to point out into the solvent as a noodle, such that it was not included in the predicted protein structure docking.

Aggregation kinetics of CsgA using thioflavin T (ThT), indicate a concerted sigmoid behaviour with an exponential rise to a plateau within 10 hours. We have replicated these ThT kinetics with our CsgA constructs as well (see Figure 2B). Previous published circular dichroism with ThT kinetics, reports an IDP before aggregation (*21*), Thus, the exploration of CsgA's folding process before aggregation is warrented. Single molecule methods with OT offer *in vitro* measurements in desired buffer and temperature conditions for down to angstrom resolution with picoNewtons (pN) of force (*31*). OT and other single molecule methods can also be leveraged to probe the dynamics and interactions of proteins within complexes (*32*). Our work herein focuses on the folding pathways and intermediate states revealed by OT, which were previously hidden at the ensemble level.

Results

Controlling the onset of fibrillation was important for producing CsgA linked with dsDNA for single molecule measurements. We used CsgA with internal cysteines and with ybbR linkers on its flanks (see table 1) for which fibrillation is impeded when the disulfide bond is intact. The ybbR tags allowed for enzymatic attachment (Sfp) to CoA-DNA handles, which were linked to functionalised beads in a dumbbell arrangement.

Both the wild type CsgA and that with residue substitutions A63C & V140C were purified using FPLC then tested for fibrillation propensity with ThT fluorescence and amyloid fibrils compared under transmission electron microscopy to verify its similarity (see Figure 2). The introduction of a reducing agent quickly led to the exponential growth curve of amyloid fibrils (Figure 2B).

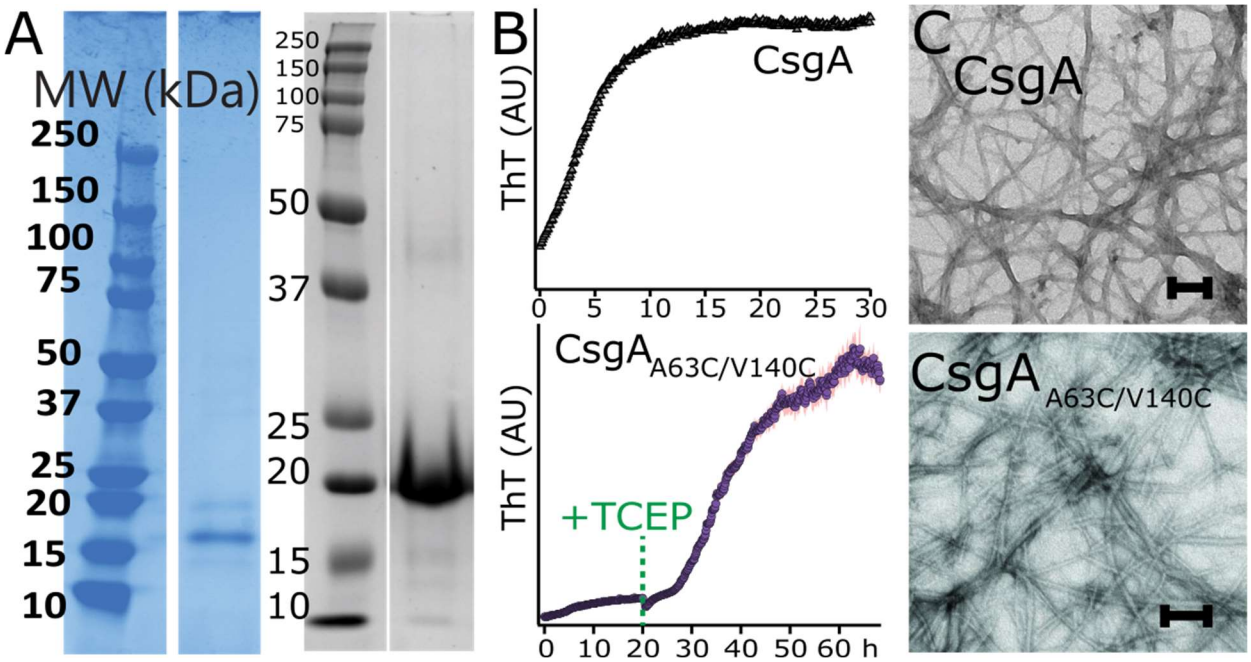

Figure 2 **Purification and qualification of CsgA**. **A**: SDS-PAGE of wild type (left) and mutant (right) CsgA. **B**: Aggregation kinetics from thioflavin T (ThT) binding fluorescence (AU) of CsgA wt (top) and mutant CsgA (bottom). **C**: TEM microscopy of wt (top) and mutant (bottom) CsgA (scale bar 100 nm).

CsgA constructs were initially screened for a single tether in running buffer without reducing agent. The data was fit offline to a worm-like chain (WLC) (*33*) to confirm that it was a single tether (Figure 3A). Before reduction, with the internal disulfide intact, force extension curves (FECs) were smooth with no apparent transitions. After the addition of a reducing agent (Figure 3B inset), the FECs showed transitions and a total contour length consistent with the length of the dsDNA plus reduced protein construct. The unfolding of CsgA showed two different qualitative behaviours, the first was large and discrete unfolding events consistent with the β-solenoid made up of β-sheets arranged into hairpins for each R domain, as shown in modelling in the literature as well as by RoseTTAFold and AF3. The other pattern was of a lower force unfolding, often without discrete steps and with greatly reduced hysteresis of refolding vs unfolding FECs. Examples are

shown in Figure 3B, 4B with WLC fit lines. In Figure 3, the process of disulfide bond reduction is illustrated: when a reducing agent was introduced, accomplished by moving the dumbbells into a flow channel where mercaptoethylamine (MEA) is in solution, at which point when the cysteines were reduced, the contour length of flexible polypeptide increased significantly, producing a notable elongation in the FEC, and then subsequent unfolding FECs may show discrete evens characteristic of cooperative R domain unfolding. However, while not in a reducing buffer, CsgA would occasionally show a small unfolding event; see Figure 3C. In Figure 4A we present a general unfolding example for CsgA, from all R domains folded together to the molecule fully unfolded. In this example, divergence from the R1-R5 fit line was seen, as well as with the subsequent FEC that happens to finally unfold from approximately 3.5 R domains instead. A rough shoulder feature appeared in the FECs before large unfolding events, where the contour length change from WLC fittings indicates the involvement of the N22 domain.

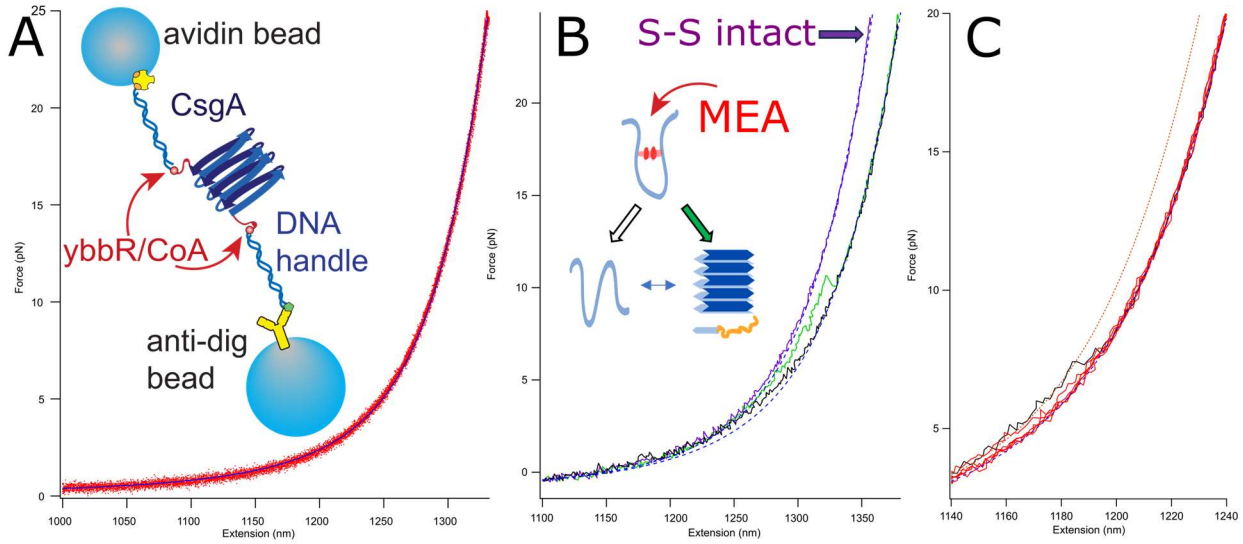

Figure 3 **Example single molecule FEC of CsgA**. **A**: initial overlaid force extension curves (FECs) without reducing agent and an intact disulfide bond, engineered to trap CsgA in a disordered or non-amyloid fibril competent state. A WLC fit used to screen for single tethers is overlaid. Inset: diagram of CsgA with linkers to dsDNA handles (not to scale). **B**: Inset: addition of reducing agent MEA to break the disulfide bond and thus reproduce wild type CsgA folding behaviour. In violet, the FEC with the bridge intact, fit with 35.1 nm of free polypeptide, then black fully unfolded refolding FEC with 62.5 nm of free polypeptide. In green, unfolding FEC with cysteines reduced. **C**: Structure of intact disulfide bridge CsgA: occasionally a 10-13 nm unzip is seen before the introduction of a reducing agent, which is consistent with the free regions of R1 and R5 outside of the disulfide looped structure containing R2, R3 and R4.

We analysed eight CsgA molecules with over 200 pulls overall, examining the effects of pulling velocities (50, 100 and 200 nm/s) and refolding times at low force (200 ms to several seconds) on unfolding of CsgA. Results of FEC behaviour are summarised in the scatterplot in Figure 4B. Unfolding data from less discrete FECs is omitted here, but it falls generally in the 4-8 pN range.

All discrete unfolding events are reduced to histogram form to look for clustering, in bins of 1 nm for contour length change and 1 pN for unfolding force in Figure 5. The clustering of events between 5 and 10 pN was also the non-discrete un- and re-folding range seen in our FECs.

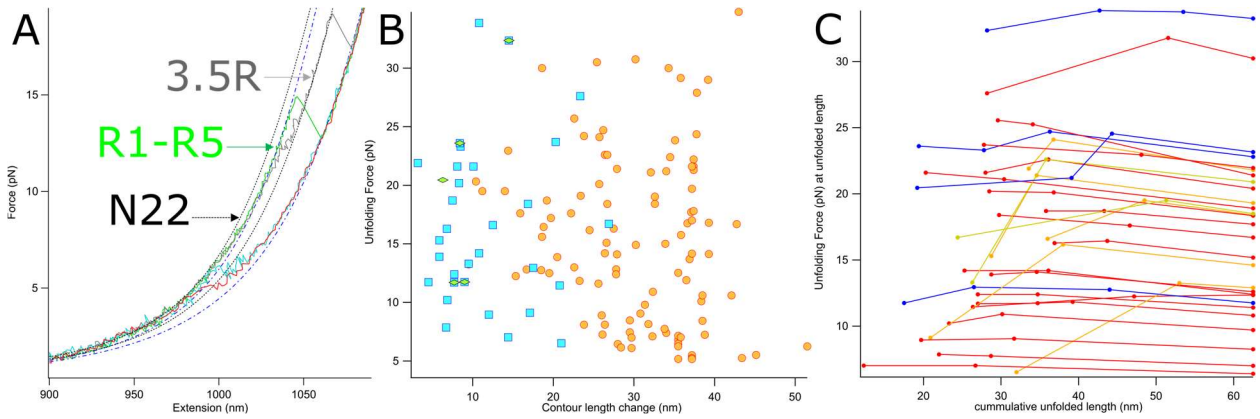

Figure 4 **Characteristic CsgA force-extension curve behaviour, discrete unfolding forces vs contour length changes**. **A**: Example FECs showing discrete unfolding of states: R1 through R5 in green, approximately 3.5 R domains in grey. While another unfolding FEC in cyan went through a rough unfolding process, very close to a characteristic refolding FEC in red. WLC fits for the fully unfolded state and for R1-R5 are shown as blue dashed lines. The range to the N22 region is in dashed black, as is the upper ~3.5R fit. The beads were moved apart at a constant velocity of 200 nm/s, with a 200 ms refolding time between sequential curves. **B**: The last discrete unfolding event data from all the FECs (orange circles), as with the example in panel 4A is shown in the scatterplot. Contour length changes from two and three state unfolders: first of three in green diamonds, first of two and second of three states in blue squares. **C**: Discrete unfolding paths of CsgA**.** In FECs tabulated from four molecules, multiple discrete unfolding steps can be observed (three distinct states in blue), up to the point where they unfold to 62.5 nm, which is the fully unfolded length of the CsgA construct. The protein starts out with 15.3 nm of unstructured polypeptide. (Much of the contour length change from the fully folded state may not occur discretely, and thus not shown here.)

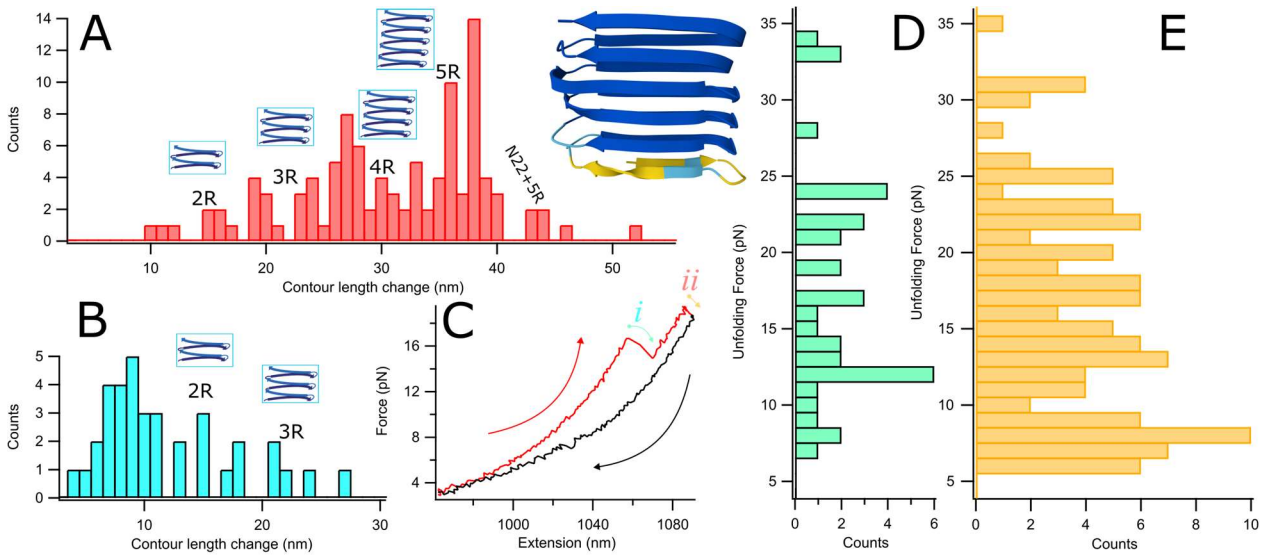

Figure 5 **Clustering of unfolding force vs contour length change of unfolding events**. **A**: Histogram of contour length change from last or only discrete unfolding event. Inset: CsgA prediction from AF3 with N22 domain in yellow and light blue, showing the weak prediction of β sheets. **B**: Contour length changes of primary unfolding events, preceding final unfolding events. **C:** Example FEC of stepwise CsgA unfolding as two discrete steps, which contributes to the histograms in A and B. In red is the unfolding FEC, while the immediate refolding FEC is in black, and then the primary unfolding event, *i*, followed by final discrete unfolding, *ii*. **D:** Histogram of primary unfolding forces corresponding to B, in light green. **E**: Histogram of final unfolding forces of discrete events corresponding to A, in yellow.

A limited number of FECs also showed two or three *strongly discrete* unfolding steps on their path to becoming fully unfolded, as shown in Figure 4C. The unfolding length change goes from an unstructured 15.3 nm (accounting for ybbR and GSSS spacer sequences to dsDNA) to a fully unfolded length of 62.5 nm. Most transitions are fairly flat in term of unfolding force, meaning that they typically occur in a very short period after the initial contour length change, though there were significant increases in force that occur less frequently.

In FEC samples from a refolding time limit of 200 ms, only 11 of 46 curves (24%), had final unfolding events classifiable as discrete. With a refolding time-limit of 500 ms, this rate rises to 33 of 42 (79%), though nine of these are within 10 pN that overlaps with the non-discrete folders, and with a 1 s refolding time the rate stays similar at 37 of 50 (74%). We have fewer curves restricted to a 2 s refolding time, showing a 16 of 22 (73%) discrete unfolding rate. In one outlier, a non-discrete state is seen after 53 s to refold, but generally, longer waiting times for refolding often show a discrete unfolding event.

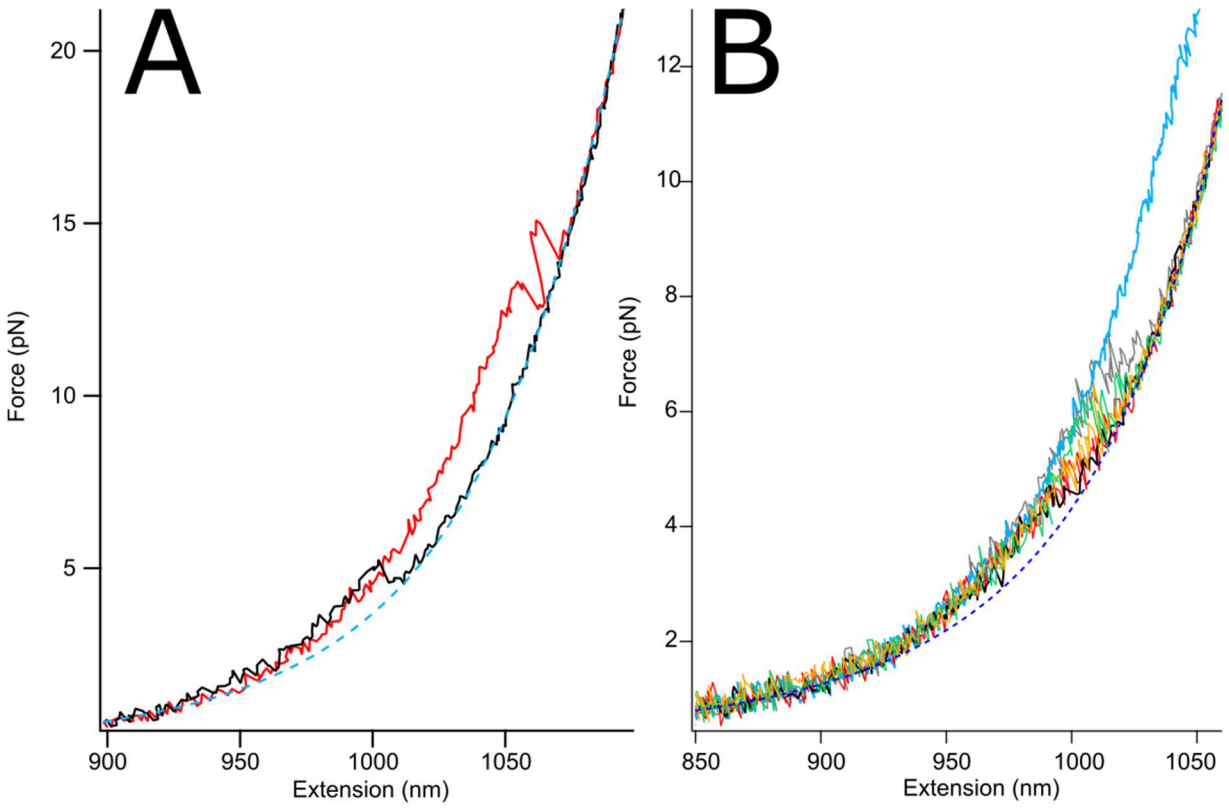

Figure 6 **State switching and metastability in FECs**. **A:** In this example, we have a molecule that unfolded at 13.9 pN yielding 20.5 nm to the fully unfolded state but switched back into an unfolded state breaking momentarily at 15.6 pN, yielding 18.6 nm. Unfolding curve in red, subsequent refolding in black, WLC for the unfolded state in light blue. **B**: Metastability of CsgA: all our refolding FECs pass through a subtle shoulder, but more than 20% of unfolding FEC did not display a *lasting* discrete behaviour near the refolding region. The bright blue FEC here shows a discrete unfolding of ~3.5 R domains at ~18pN, to the fully unfolded WLC fit dashed dark blue line, with an example refolding FEC in black. Other unfolding FECs in grey, green, orange and red oscillated between short extension with varying length. Data in panel B is from a 100 nm/s ramp with a 200 ms refolding pause at zero force.

Refolding and unfolding were also not always observed to be in one direction with the ramping of force. Typically, state switching was observed at forces between 4 to 10 pN, but this phenomenon has been observed as high as 15 pN, as shown in Figure 6A, with a 200 nm/s ramp. (Faster loading rates are farther from equilibrium.) Across all our refolding curves a "shoulder" was observed where the trace diverges from a WLC (Figure 6B). Importantly, in curves that cannot be assigned a clear lasting discrete unfold, a rough trace occurred, rather than the monotonic rise usually seen with dsDNA or with our CsgA pinned with a disulfide bond (Figure 3C). Currently our time resolution limits vary from ~5 to 7 ms per data point.

In order to characterise the non-discrete FEC, we used a model that describes sub-states in rapid equilibrium (see eqn 2). This model has previously been used to characterise phenomenologically similar proteins studied by SMFS: α-synuclein (*25*) and prion protein dimer (*24*). We limited the

number of free parameters of the fitting function, while considering three independent metastable states to: the N22 region, with two and three R domains. Non-discrete curves were aggregated together for sets of identical trap velocities and refolding times. Both data masks for fit restriction and overall data binning were used with the fitting function (see Figure 7A, B). The most persistent state with respect to applied force is a multiple of two R domains, with three R domains preceding at lower force. The equilibrium force, $F_{1/2}$, trends upwards both with trap velocity and refolding time within our sampling range (see Figure 7C). The metastable transitions before discrete unfolding events is well described by the rapid equilibrium model, with an example shown in Figure 7D. FEC curve hysteresis is subtle when comparing many of these non-discrete curves to the refolding, but quantifiable, as shown in Figure 7B.

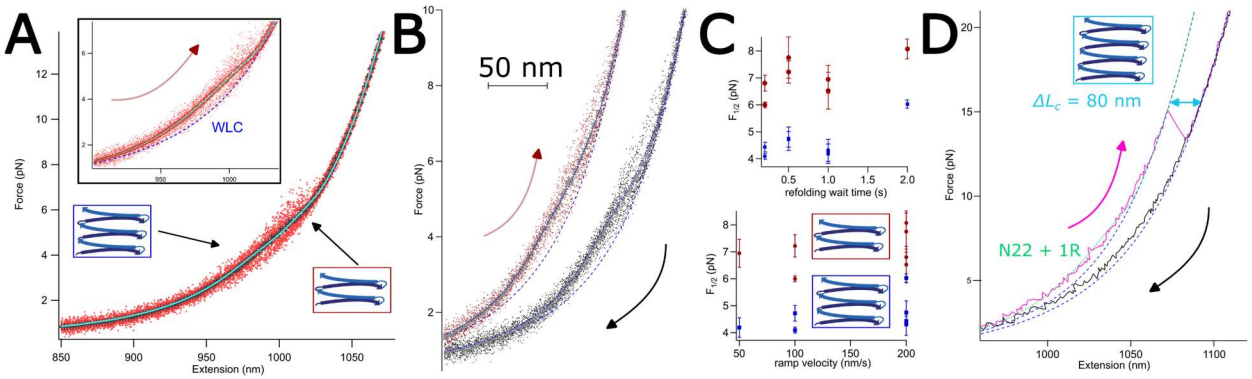

Figure 7 **Fitting metastability in FECs**. **A:** Example case of non-discrete FECs with 200 ms of refolding time and a trap velocity of 100 nm/s. With three states considered in rapid equilibrium, the FECs can be weighed by the N22, 3R and 2R using eqn 2. 2R persist with an $F_{1/2}$ of 5.9 pN, while 3R has a lower $F_{1/2}$ of 4.2 pN. Inset: the WLC without inclusion of eqn 2 for rapidly changing states is overlaid as the broken line in blue. **B:** Comparison of 200 nm/s complementary unfolding (red) and refolding (black) aggregate data; visually separated by 50nm. Here the higher force 2R state has an $F_{1/2}$ of 7.3 pN when unfolding and of 5.8 pN when refolding, while 3R has a similar $F_{1/2}$ of 4.5 vs 4.1 pN, respectively. **C:** The $F_{1/2}$ for both mid-range 3R (blue) and higher force range 2R (red) generally both increase as a function of trap velocity (bottom) and refolding time (top). **D:** Discrete FEC with metastable state lead-in. Consistent with aggregated non-discrete FEC fitting, the model here considers the N22 ($F_{1/2}$ of 5.4 pN) and a single R domain ($F_{1/2}$ of 8.9 pN) in rapid equilibrium, before four R domains unfold cooperatively at 15.1 pN.

Discussion

It has been reported in the literature that CsgA undergoes conformational rearrangement from an initially soluble, intrinsically disordered monomer to form a β-sheet rich amyloid through an unknown mechanism. The first steps of nuclei formation are hypothesized to include either transient folding of two CsgA monomers that then bind together to form the amyloid nucleus, or co-operative binding and folding of two CsgA monomers to form structured dimers (*18*).

Following CsgA protein synthesis in *E. coli*, the signal peptide is cleaved, leaving the five R domains as well as 22 residues on its N terminus (N22), which is then exported out of the cell before forming fibrils nucleated by CsgB. It has been assumed that CsgA is maintained as an IDP in the cell until fibril assembly, and immediately after purification, published circular dichroism spectra data show predominantly random coil before fibril growth (*34*). Close examination of our data show that around ~73-79% of FECs yield weak, non-discrete, folding and refolding that could be described as a molten globule or a metastable fold (e.g. in Figures 3, 6 and 7). Moreover, the data gap (0-10 pN, 10-20 nm) in Figure 4 due to this metastable protein state we observe, where phenomenologically gradual or non-cooperative length changes occur (detailed in Figure 7). Clustering of contour length changes can be seen at 20, 27 and 37 nm, which can be attributed to 3, 4 and 5 R domains, respectively, as shown in Figure 5. Importantly, many contour length changes appear to involve half multiple R domain as well, e.g. 3.5 R domains in Figure 4A. The unfolding of half of an R domain could be interpreted as the result of the shearing of a β-hairpin. What can be seen from the discrete step unfolding data of Figure 4C is that most of these folded states have a limited lifetime, and rapidly unfold at close to the same force value. Lastly, a piecewise or sequential unfolding of R domains was never observed.

The non-monotonic rise of our FECs, with a "shoulder"-like deviation from the WLC is an important nuance. This metastable behaviour of CsgA seen in 20 to 25% of FEC we attribute to a metastable or molten-globule quality of CsgA, and it is distinct from the observations of the IDP α-synuclein "shoulder" reported by Solanki *et al.* (*25*, *26*) where they described a monotonic rise without observable fluctuations. However, the model of rapidly fluctuating states (eqn 2) used to fit the α-synuclein shoulder applies well with our CsgA FECs. CsgA appears to have a more intermediate behaviour between something like α-synuclein and CsgA's stable or trapped structure present in amyloid fibrils. The fluctuations in CsgA's shoulder are more extensive than those seen with prion dimer (*24*). Examination of a hydropathy plot for CsgA shows significant hydrophilicy, suggesting competition between forming hydrogen bonds with itself and with the solvent, and perhaps that entropy maximisation keeps CsgA metastable. Hansen *et al.*'s studies of the CsgA homologue FapC suggests several folding states, from secondary structure alone, then to small scale cross-β structure before conformational changes adjusting the folded monomer to the distinct fibrillar fold; based on data combining NMR, cryo-EM and MD simulations (*30*). Additionally, in our CsgA data, the N22 region participates in this shoulder and occasionally appears to be included in a discrete unfolding structure. AF3 predicts a complementary β-strand to R1 with a plDDT between 50 to 90 (depending on the prediction run) within the N22 region as well. Partial β-sheet stacking from the N22 region with R1 does not fit into the observed amyloid fibril structure (*20*). Ongoing work in our research group is examining a truncation mutant of CsgA with this region removed.

Our metastable region shows behavioural similarity, qualitatively, to the observations of apomyoglobin measured at pH 5 by Elms *et al.* (*35*), where they reported that a large transition state distance $\Delta x^{\ddagger}$, as described by Bell's equality $k = k_{off} \exp[(F\Delta x^{\ddagger})/k_B T]$ (*36*). They describe the

molten globule state as compliant, permitting large fluctuations in end-to-end extension without crossing the folding barrier, but with the folding rates are more sensitive to force. To quantify this molten globule in equilibrium, they used constant trap separation, and then populate the states in force distributions. With continued work, it will be possible to further explore the interplay of secondary structure within CsgA using force spectroscopy in equilibrium experiments.

It may be equally appropriate to describe CsgA as having a mechanically labile regime, given that it is secreted by β barrel CsgF-G pore complex out of the cell. For instance, low mechanical stability may be useful for protein secretion through the pore complex of T3SS – though this is in the context of atomic force microscopy (AFM), where low force is in the region of 15-20 pN (*37*). LeBlanc *et al.* also show a trend towards a larger transition state distance with increasing mechanical lability.

Another protein study within the regions of low force metastability or equilibrium similar to CsgA measured under equivalent conditions, Jahn *et al*. report a report a switching behaviour at ~ 5 pN due to a 61 amino acid charged linker between the protein Hsp82 N- and M- domains hopping between a compact and extended conformation, described as reversible folding and unfolding (*38*, *39*). (Though they do not use terms such as metastable). When they mutated out the charged linker with unstructured glycine-glycine-serine repeats, their low force fluctuations vanished within the resolution of their instrumentation. Jahn *et al.* also discuss the linker as only having secondary structure, given that they have examined the charged linker's behaviour with constant trap separation experiments (*5 min clamping periods*). The differentiation of CsgA's discrete and metastable unfolding pathways could be well described as the difference between secondary structure along and its compaction into a structure with tertiary features; the latter of which may well be amyloidal.

Yet another similar behaviour can be found in the work of Alexander *et al.*, where they report reversible refolding of the calerythrin protein and the EF-hands 3 and 4, where each is an α helix-loop-helix motif with a Ca^{2+} binding site (*40*), but importantly, they reports its unfolding as always discrete.

Experiments here have two compromises that limits the lifetime of our samples and the forces that can be applied. The ssDNA-CoA oligo attached to the protein of interest are merely annealed to the overhang of the dsDNA handles without ligation (*see Materials and Methods for more detail*). In practice, this means limiting forces to within 40 pN of applied tension of the handles, because high force leads to oligo shearing from the overhang. For instance, five pulls of CsgA did not show unfolding within 200 ms at 25 or 30 pN during initial screening. The second challenge is the targeted reduction of the internal cysteine disulfide bridge. Aggregation kinetics of this construct were demonstrated with ThT binding (see Figure 2B), triggered by the introduction of tris(2-carboxyethyl) phosphine (TCEP). However, TCEP is too strong a reducing agent to incubate with anti-dig functionalised beads, as immunoglobulin G (IgG) has structural disulfide bonds. Instead, MEA is carefully introduced, chosen because it is known selectively to reduce the hinge region of IgG, leaving antigen binding sites and Fab regions intact. However, some softening of the IgG was indicated by a minor drop in the modelled persistence length and 30% in the modulus of the WLC.

The observation of structure of R1 & R5 partial regions with A63C/V140C disulfide bridge intact: During screening, most tethers in the absence of reducing agent show no unfolding events during pulling, however, occasionally an unzip of 10 to 13 nm in the ~5 to 7 pN range was notable (Figure 3C). Outside of the disulfide bridge at 63C and 140C, R1 and R5 have 32 free amino acid

residues, which normally would be part of the β-hairpin structure of their respective R domain. Residues 64 through 139 are bound into a loop with no structure prediction available. Balistreri *et al.* hypothesized that the disulfide bridge keeps the CsgA in a disordered state (*14*), but the rapid onset of fibrillation of CsgA A63C/V140C after the introduction of a reducing agent (TCEP) suggests to us that some seeding aggregates may already be possible. OT results indicate, typically on a first pull alone, that a partial β-hairpin or β-sheet formation sequestering these 32 free residues is possible given the change in contour length. AF3 and RoseTTAFold do not offer a structure prediction with the disulfide intact.

In order to better interpret and understand the unfolding behaviour of CsgA under tension when pulled by optical tweezers, preliminary steered molecular dynamics simulations (LAMMPS) have also been undertaken by our collaborators (K. Kudriavtsev & S. Srebik). They were guided by the work of DeBenedictis and Keten (*41*), with the AF3 predicted structure as a starting point. Contact maps show a dominance of parallel β-sheets under tension with the transient formation of antiparallel β-sheets on the ends of the central R domains, as R3 is the last to unfold. Moreover, the tracking of contact ratios shows those from R2 to R3 being the most persistent. At the high loading rate present in simulations, shearing of the protein structure is a prominent feature. In our FECs, the odd half integer R domain ratios appear to be a reflection of this shearing. By contrast, any IDP, molten-globule or metastable form of CsgA is not modelled by these simulations. The molecular dynamics simulations must start from a compact structure provided by a PDB structure, such as the cryoEM result or an AF3 prediction, and importantly, they must be limited to the nanosecond time scale due to computational costs. As such, these simulations are best applied to relatively high force discretely unfolding FECs of CsgA, namely the results of Figure 4.

Conclusions

We have reported the first single molecule folding data of CsgA, based on hundreds of FECs, which presents a unique blend of metastable - molten globule behaviour and cooperative unfolding consistent with the R domains modelled within the structures found within amyloid fibrils imaged by cryoEM. The R domains are a fixture of discrete unfolding of CsgA, while β hairpin secondary structures appear to be present in metastable unfolding pathways. In other words, the CsgA protein does not appear to be locked into an amyloid subunit form while present as a monomer in solution. This is in contrast to the assumption from ensemble experiments, such as circular dichroism, pointing towards an intrinsically disordered state. Moreover, a piecewise unfolding of CsgA by R domain or β hairpin is never observed. Instead, evidence points towards partial shearing of β hairpins and partial metastability. Equilibrium measurements with optical tweezers could produce more insights into dominant folding pathways of the metastable state of CsgA. There are engineered mutations of CsgA worth investigating further, namely the 'slowgo' mutant (*42*) and clarifying if the N22 region modifies protein fold stability.

Materials and Methods

Protein expression: C-terminal His_6-tagged CsgA (A63C, V140C) was expressed and FPLC purified as previously described with some modifications (*18*, *43*, *44*). NEB 3016 ΔslyD cells harboring a pET11d vector encoding C-terminal His_6-tagged CsgA were grown to $OD_{600} \gtrsim 1$ in

LB broth containing 100 µg/mL ampicillin at 37°C. CsgA expression was induced with 0.5 mM IPTG for 2-3 h, then cells were harvested (8000 rpm, 10 min) and finally stored at -80°C. Cell pellets from 1 L of the induced cell culture were resuspended in 20 mL lysis buffer (8 M GdnHCl, 50 mM K_2HPO_4, pH 7.3) per gram of pellet, sonicated for a few min (20 s intervals), and shaken for 1 h at RT. The supernatant of the cell lysate was collected following centrifugation ($4 \cdot 10^4 \times g$ for 40 min), then mixed with an equal volume of equilibration buffer (50 mM Na_2HPO_4, 300 mM NaCl, 6 M GdnHCl, 10 mM imidazole, pH 7.4) and then purified using FPLC and a *HisPur* Cobalt column (Cytiva). Protein was eluted (6 M GdnHCl, 50 mM Na_2HPO_4, 300 mM NaCl, 150 mM imidazole, pH 7.4). Fractions containing CsgA were pooled together and stored at 4°C prior to analysis. All purification steps were conducted under 6 M GdnHCl to prevent premature fibrillation. See Figure 2A for PAGE gel purification results.

Aggregation kinetics: In order to minimise the aggregation time in native conditions, Zeba desalting columns (Thermo Scientific) were used to quickly buffer exchange the CsgA protein from 6 M GdnHCl into 50 mM HEPES buffer at pH 7.0. Thioflavin T (ThT) was added to a concentration of 20 µM before the sample was placed into a 96 well plate for bottom reads with a SpectraMax Gemini EM (Molecular Devices) with excitation at 450 nm and emission at 495 nm, 15 reads per cell, and five replicates without shaking. Tris(2-carboxyethyl) phosphine (TCEP), used to reduce the internal disulfide, was made into a pH 7 stock in HEPES because of TCEP's acidity.

Bioconjugate Chemistry: SMFS requires extensive use of bioconjugate chemistry to connect the molecule(s) of interest, DNA handles and beads together to form 'dumbbell tethers' to keep the trapped beads far enough apart to avoid interference. As CsgA contains no native cysteines, thiol chemistry can be used to attach DNA handles, however, this would preclude the use of the internal cysteine amino acid change (*14*) that can be use to pin the protein in a metastable, disordered or non-fibril forming state. Therefore, we made use of ybbR attachment chemistry (*45*) with the commercial kit provided by Lumicks (Netherlands). The kit has ssDNA CoA-oligos of 36 nt, with complementary-overhang handles of 1506 bp on both flanks of the protein. The oligo labelled CsgA was annealed with the complementary biotin and digoxigenin handles at 37°C for 15 minutes, then the construct was diluted ~100 fold before being incubated with 2.08 µm anti-dig beads (Spherotech). Lumicks reports their handles can reach 40-45 pN before melting of the overhang/oligo, which has a GC content of 58%. In practice forces near 40 pN were avoided as this reduces tether lifetime.

SMFS – dumbbell fishing with 1.14 µm streptavidin beads (Spherotech) was performed within a five-channel microfluidic flowcell of the Lumicks C-trap (dual beam/trap optical tweezers). Bead position within the traps was recorded using back focal plane detection with position sensitive detectors and sampled at 78.125 kHz with an NI-4472 acquisition card (National Instruments) with 64× anti-aliasing (5 MS/s per channel). Beam steering is dependent on a piezo-mirror driven by a Mad City Labs 20-bit Nano-Drive, with a driving loop of 80 Hz in steps of 5 to 10 nm. This precludes the use of a closed loop control (e.g. proportional–integral–derivative controller) for constant force experiments, since CsgA's folding dynamics are faster than 6 ms, as observed with our force extension curves. Therefore, equilibrium experiments can only be done by constant trap separation. Data was imported into Igor Pro 9 (Wavemetrics), where it was down-sampled to millisecond time resolution with appropriate filtering for anti-aliasing. Force extension curves (FECs) were extracted then with two worm-like chains (WLCs) in series as described previously (*24*). In the WLC, force, F and change in extension, Δx, takes the function form:

$$F(\Delta x) = \frac{k_B T}{L_p}\left[\frac{1}{4}\left(1 - \frac{\Delta x}{L_c} + \frac{F}{K}\right)^{-2} - \frac{1}{4} + \frac{\Delta x}{L_c} - \frac{F}{K}\right], \qquad \text{eqn 1}$$

Where k_B is the Boltzmann constant, with absolute temperature, T. The dsDNA fitting parameters have a persistence length (L_p) of ~40 nm and elastic modulus (K) of ~1000 pN, while unfolded polypeptide lengths used an L_p of 0.85 nm, a K of 2000 pN and the crystallographic contour length of amino acids L_c/a.a. = 0.36 nm, for conversion to involved residues (*24*). The length between R domains of 4.8 Å, as well as full dimensions consider both the cryoEM results (*20*) and simulations (*28*), are all used to determine the inter-termini distances included for unfolding events.

The disulfide bridge of the CsgA (A63C/V140C) was broken using ~100 mM MEA (MercaptoEthylAmine) in a fourth channel of the microfluidic cell. However, the compliance of the handles changes due to partial reduction of disulfides of the IgG, depressing the modulus to ~700 pN when fitting the handles with the WLC. After establishing the break of the internal disulfide bridge, the dumbbell was moved back into a running buffer of PBS with an oxygen scavenging system as previously described (*24*) with 50 U/mL glucose oxidase (GOx), 140 U/mL catalase and 0.01% D-glucose, as well as 10-20 mM of MEA to keep the protein's cysteines reduced. MEA levels need to be moderated as GOx (*A. niger*) has a disulfide bond between residues 164 and 206 required for enzyme function (*46*), though our catalase (bovine) is not known to require disulfide bridges for enzymatic function.

***Analysis**:* Force extension curves (FECs) were fit using the worm like chain (WLC) model from Marko and Siggia encoded in Igor Pro (Wavemetrics). The Lumicks OT instrument (C-trap) uses two traps by polarisation splitting and then back focal plane detection with position sensitive devices (PSDs). When the two trapped beads are close together deflected beams produce secondary spots on the detectors. This crosstalk is very similar to a Bessel function of the first kind seen with an Airy disc. Given the trapping wavelength of 1064 nm (λ), this crosstalk is quite strong within one λ of the bead contact surfaces. The curvature of the FECs is very sensitive to this correction (subtraction of a large polynomial fit), but when done carefully, we maintain a persistence length (Lp) of ~40 nm and a modulus (K) of ~1000 pN for dsDNA. Without detection scheme modification this crosstalk can be further addressed with smaller beads (~1 µm pair) (*47*) and longer dsDNA handles.

For the shoulder-like metastable features of the CsgA FECs, we have transitions that are both faster and on a similar timescale as data sampling and filtering of our instrumentation. We make use make use of the minimal model that assumes independent structures with two state transitions in rapid equilibrium, which has previously been successfully applied to α-synuclein (*25*) and prion dimer (*24*):

$$x(F) = x_H(F) + x_U(F) + \sum_{i=1}^{n} P_u^i(F)\,\Delta\, x_i(F), \qquad \text{eqn 2}$$

Where $x_H(F)$ is the extension of the dsDNA handles, $x_U(F)$ is the extension of the unstructured region of the protein, n is the number of two state structures with distinct unfolding properties. Alternatively, if several two state structures have similar unfolding properties, as seen with α-synuclein multimers (*25*), this can be written as:

$$x(F) = x_H(F) + x_U(F) + \sum_{i=1}^{n} N_i \cdot \left[P_u^i(F)\,\Delta\, x_i(F)\right],$$

Where N_i represents the number of similar structures. For two-state unfolding in equilibrium, the probability term is described as:

$$P_u^i(F) = \{1 + \exp[(F_{1/2}^i - F) \cdot \Delta x_i(F)/k_B T]\}^{-1}$$

Where $F_{1/2}^i$ is the force at which the structure has a 50% probability of being unfolded, with the corresponding extension change for that structure $\Delta x_i(F)$. Forces here correspond to those of the WLC used to fit the dsDNA handles and determine the contour length change from discrete transitions.

Table 1 CsgA construct sequence.

ybbR and linker sequence	MDSLEFIASKLAGGGGSGGGGS
N22 (21-42)	GVVPQYGGGGNHGGGGNNSGPN
R1 (43-65)	SELNIYQYGGGNSALALQTD**C**RN
R2 (66-87)	SDLTITQHGGGNGADVGQGSDD
R3 (88-110)	SSIDLTQRGFGNSATLDQWNGKN
R4 (111-132)	SEMTVKQFGGGNGAAVDQTASN
R5 (133-151)	SSVNVTQ**C**GFGNNATAHQY
Linker, ybbR and His tag sequence	GGGGSGGGGSDSLEFIASKLAGGGGSGGGGSHHHHHH

Acknowledgements

We have many colleagues to thank who supported this work in some way or another. In particular, Prof. Matthew Chapman and Anthony Balisteri, who shared details about their research panel of engineered mutants for CsgA and their *E. coli* cell strain for expression. Adaptation and additional development of the expression protocol was done by Fan Bu (our first liaison with A. Balisteri), who also continues to provide insights into CsgA amyloid formation. The internal cysteine mutant was developed by A. Balisteri. Our summer undergrads Hrishika Dekate and Rachel Rosenberg worked on protein expression used for experimental assays such as ThT kinetics and TEM results.

Prof. Johannes Stigler graciously shared his C-trap HDF5 import code for Igor. Additionally, Noel Hoffer (Lumicks) provided helpful discussions about instrument operation and bead optimisation, while Krishna P. Neupane offered helpful discussions in regards to handle length and trap crosstalk.

References

1. N. Jain, M. R. Chapman, Bacterial functional amyloids: Order from disorder. *Biochimica et Biophysica Acta (BBA) - Proteins and Proteomics* **1867**, 954–960 (2019).

2. N. Van Gerven, R. Klein, S. Hultgren, H. Remaut, Bacterial amyloid formation: structural insights into curli biogensis. *Trends Microbiol* **23**, 693–706 (2015).

3. D. Romero, C. Aguilar, R. Losick, R. Kolter, Amyloid fibers provide structural integrity to Bacillus subtilis biofilms. *Proceedings of the National Academy of Sciences* **107**, 2230–2234 (2010).

4. J. Li, F. Zhang, Amyloids as Building Blocks for Macroscopic Functional Materials: Designs, Applications and Challenges. *International Journal of Molecular Sciences* **22**, 10698 (2021).

5. M. R. Chapman, L. S. Robinson, J. S. Pinkner, R. Roth, J. Heuser, M. Hammar, S. Normark, S. J. Hultgren, Role of Escherichia coli Curli Operons in Directing Amyloid Fiber Formation. *Science* **295**, 851–855 (2002).

6. S. K. Collinson, J. M. R. Parker, R. S. Hodges, W. W. Kay, Structural predictions of AgfA, the insoluble fimbrial subunit of Salmonella thin aggregative fimbriae11Edited by W. Baumeister. *Journal of Molecular Biology* **290**, 741–756 (1999).

7. S. K. Collinson, L. Emödy, K. H. Müller, T. J. Trust, W. W. Kay, Purification and characterization of thin, aggregative fimbriae from Salmonella enteritidis. *Journal of Bacteriology* **173**, 4773–4781 (1991).

8. F. Shewmaker, R. P. McGlinchey, K. R. Thurber, P. McPhie, F. Dyda, R. Tycko, R. B. Wickner, The Functional Curli Amyloid Is Not Based on In-register Parallel β-Sheet Structure *. *Journal of Biological Chemistry* **284**, 25065–25076 (2009).

9. M. S. Dueholm, D. Otzen, P. H. Nielsen, Evolutionary Insight into the Functional Amyloids of the Pseudomonads. *PLOS ONE* **8**, e76630 (2013).

10. A. Bleem, G. Christiansen, D. J. Madsen, H. Maric, K. Strømgaard, J. D. Bryers, V. Daggett, R. L. Meyer, D. E. Otzen, Protein Engineering Reveals Mechanisms of Functional Amyloid Formation in Pseudomonas aeruginosa Biofilms. *Journal of Molecular Biology* **430**, 3751–3763 (2018).

11. K. H. Hansen, C. H. Byeon, Q. Liu, T. Drace, T. Boesen, J. F. Conway, M. Andreasen, Ü. Akbey, Structure of biofilm-forming functional amyloid PSMα1 from Staphylococcus aureus. *Proceedings of the National Academy of Sciences* **121**, e2406775121 (2024).

12. N. D. Hammer, J. C. Schmidt, M. R. Chapman, The curli nucleator protein, CsgB, contains an amyloidogenic domain that directs CsgA polymerization. *Proceedings of the National Academy of Sciences* **104**, 12494–12499 (2007).

13. J. D. Taylor, W. J. Hawthorne, J. Lo, A. Dear, N. Jain, G. Meisl, M. Andreasen, C. Fletcher, M. Koch, N. Darvill, N. Scull, A. Escalera-Maurer, L. Sefer, R. Wenman, S. Lambert, J. Jean, Y. Xu, B. Turner, S. G. Kazarian, M. R. Chapman, D. Bubeck, A. de Simone, T. P. J. Knowles, S. J. Matthews, Electrostatically-guided inhibition of Curli amyloid nucleation by the CsgC-like family of chaperones. *Sci Rep* **6**, 24656 (2016).

14. A. Balistreri, D. Kolli, S. W. Jayaweera, D. Lundahl, Y. Han, L. Kalcec, E. Goetzler, R. Alessio, B. Ruotolo, A. Olofsson, M. R. Chapman, The bacterial chaperone CsgC inhibits functional amyloid CsgA formation by promoting the intrinsically disordered pre-nuclear state. *Journal of Biological Chemistry* **301** (2025).

15. L. Sewell, F. Stylianou, Y. Xu, J. Taylor, L. Sefer, S. Matthews, NMR insights into the pre-amyloid ensemble and secretion targeting of the curli subunit CsgA. *Sci Rep* **10**, 7896 (2020).

16. M. Andreasen, G. Meisl, J. D. Taylor, T. C. T. Michaels, A. Levin, D. E. Otzen, M. R. Chapman, C. M. Dobson, S. J. Matthews, T. P. J. Knowles, Physical Determinants of Amyloid Assembly in Biofilm Formation. *mBio* **10**, e02279-18 (2019).

17. W. Hawthorne, S. Rouse, L. Sewell, S. J. Matthews, Structural insights into functional amyloid inhibition in Gram −ve bacteria. *Biochem Soc Trans* **44**, 1643–1649 (2016).

18. M. Sleutel, I. Van den Broeck, N. Van Gerven, C. Feuillie, W. Jonckheere, C. Valotteau, Y. F. Dufrêne, H. Remaut, Nucleation and growth of a bacterial functional amyloid at single-fiber resolution. *Nat Chem Biol* **13**, 902–908 (2017).

19. M. Sleutel, B. Pradhan, A. N. Volkov, H. Remaut, Structural analysis and architectural principles of the bacterial amyloid curli. *Nat Commun* **14**, 2822 (2023).

20. F. Bu, D. R. Dee, B. Liu, Structural insight into Escherichia coli CsgA amyloid fibril assembly. *mBio* **15**, e00419-24 (2024).

21. X. Wang, D. R. Smith, J. W. Jones, M. R. Chapman, In Vitro Polymerization of a Functional Escherichia coli Amyloid Protein *. *Journal of Biological Chemistry* **282**, 3713–3719 (2007).

22. F. Bu, D. R. Dee, B. Liu, Reply to Sleutel and Remaut, “Structural insights into Escherichia coli CsgA amyloid fibril assembly revisited.” *mBio* **16**, e0110625 (2025).

23. K. Zhou, Y. Liu, K. Li, Y. Li, S. Wei, Y. Zhou, H. Yu, Y. Zhang, J. Lv, B. Xiao, C. Zhong, Force Spectra of a Single CsgA Molecule and Amyloid Nanofibers Assembled from Chimeric Mfp5 and CBD Proteins: Implications for a Nanomaterial Testing Machine. *ACS Appl. Nano Mater.* **5**, 1758–1766 (2022).

24. H. Yu, D. R. Dee, X. Liu, A. M. Brigley, I. Sosova, M. T. Woodside, Protein misfolding occurs by slow diffusion across multiple barriers in a rough energy landscape. *Proceedings of the National Academy of Sciences* **112**, 8308–8313 (2015).

25. A. Solanki, K. Neupane, M. T. Woodside, Single-Molecule Force Spectroscopy of Rapidly Fluctuating, Marginally Stable Structures in the Intrinsically Disordered Protein $\ensuremath{\alpha}$-Synuclein. *Phys. Rev. Lett.* **112**, 158103 (2014).

26. K. Neupane, A. Solanki, I. Sosova, M. Belov, M. T. Woodside, Diverse Metastable Structures Formed by Small Oligomers of α-Synuclein Probed by Force Spectroscopy. *PLOS ONE* **9**, e86495 (2014).

27. A. Balistreri, E. Kahana, S. Janakiraman, M. R. Chapman, Tuning Functional Amyloid Formation Through Disulfide Engineering. *Frontiers in Microbiology* **11** (2020).

28. E. P. DeBenedictis, D. Ma, S. Keten, Structural predictions for curli amyloid fibril subunits CsgA and CsgB. *RSC Adv.* **7**, 48102–48112 (2017).

29. D. E. Kim, D. Chivian, D. Baker, Protein structure prediction and analysis using the Robetta server. *Nucleic Acids Res* **32**, W526–W531 (2004).

30. K. H. Hansen, M. Golcuk, C. H. Byeon, A. Tunc, E. B. Plechinger, M. K. D. Dueholm, J. F. Conway, M. Andreasen, M. Gur, Ü. Akbey, Structural basis of Pseudomonas biofilm-forming functional amyloid FapC formation. *Science Advances* **11**, eadx7829 (2025).

31. C. Bustamante, L. Alexander, K. Maciuba, C. M. Kaiser, Single-Molecule Studies of Protein Folding with Optical Tweezers. *Annual Review of Biochemistry* **89**, 443–470 (2020).

32. A. Narayan, M. T. Woodside, Probing structural dynamics and interactions in macromolecular complexes with single-molecule force spectroscopy. *Current Opinion in Structural Biology* **93**, 103110 (2025).

33. M. D. Wang, H. Yin, R. Landick, J. Gelles, S. M. Block, Stretching DNA with optical tweezers. *Biophysical Journal* **72**, 1335–1346 (1997).

34. X. Wang, D. R. Smith, J. W. Jones, M. R. Chapman, In Vitro Polymerization of a Functional Escherichia coli Amyloid Protein. *J Biol Chem* **282**, 3713–3719 (2007).

35. P. J. Elms, J. D. Chodera, C. Bustamante, S. Marqusee, The molten globule state is unusually deformable under mechanical force. *Proceedings of the National Academy of Sciences* **109**, 3796–3801 (2012).

36. G. I. Bell, Models for the specific adhesion of cells to cells. *Science* **200**, 618–627 (1978).

37. M.-A. LeBlanc, M. R. Fink, T. T. Perkins, M. C. Sousa, Type III secretion system effector proteins are mechanically labile. *Proceedings of the National Academy of Sciences* **118**, e2019566118 (2021).

38. D. Choudhary, L. Mediani, S. Carra, C. Cecconi, Studying heat shock proteins through single-molecule mechanical manipulation. *Cell Stress and Chaperones* **25**, 615–628 (2020).

39. M. Jahn, K. Tych, H. Girstmair, M. Steinmaßl, T. Hugel, J. Buchner, M. Rief, Folding and Domain Interactions of Three Orthologs of Hsp90 Studied by Single-Molecule Force Spectroscopy. *Structure* **26**, 96-105.e4 (2018).

40. L. M. Alexander, D. H. Goldman, L. M. Wee, C. Bustamante, Non-equilibrium dynamics of a nascent polypeptide during translation suppress its misfolding. *Nat Commun* **10**, 2709 (2019).

41. E. P. DeBenedictis, S. Keten, Mechanical unfolding of alpha- and beta-helical protein motifs. *Soft Matter* **15**, 1243–1252 (2019).

42. X. Wang, M. R. Chapman, Sequence determinants of bacterial amyloid formation. *J Mol Biol* **380**, 570–580 (2008).

43. X. Wang, Y. Zhou, J.-J. Ren, N. D. Hammer, M. R. Chapman, Gatekeeper residues in the major curlin subunit modulate bacterial amyloid fiber biogenesis. *Proceedings of the National Academy of Sciences* **107**, 163–168 (2010).

44. A. Balistreri, E. Goetzler, M. Chapman, Functional Amyloids Are the Rule Rather Than the Exception in Cellular Biology. *Microorganisms* **8**, 1951 (2020).

45. M. J. Avellaneda, E. J. Koers, D. P. Minde, V. Sunderlikova, S. J. Tans, Simultaneous sensing and imaging of individual biomolecular complexes enabled by modular DNA–protein coupling. *Commun Chem* **3**, 1–7 (2020).

46. S. Ittisoponpisan, I. Jeerapan, In Silico Analysis of Glucose Oxidase from Aspergillus niger: Potential Cysteine Mutation Sites for Enhancing Protein Stability. *Bioengineering (Basel)* **8**, 188 (2021).

47. M. Freitag, S. Jaklin, F. Padovani, E. Radzichevici, S. Zernia, K. M. Schmoller, J. Stigler, Single-molecule experiments reveal the elbow as an essential folding guide in SMC coiled-coil arms. *Biophys J* **121**, 4702–4713 (2022).